

# Methods of machine learning and spatial stochastics for characterizing the 3D morphology of battery materials at various length scales

Orkun Furat<sup>1,\*</sup>, Lukas Fuchs<sup>1,\*</sup>, Donal P. Finegan<sup>2</sup>, Kandler Smith<sup>2</sup>, and  
Volker Schmidt<sup>1</sup>

<sup>1</sup> Ulm University, Helmholtzstraße 18, 89069 Ulm, Germany,  
orkun.furat@uni-ulm.de,  
WWW home page: [https://www.uni-ulm.de/  
en/mawi/institute-of-stochastics/staff/orkun-furat/](https://www.uni-ulm.de/en/mawi/institute-of-stochastics/staff/orkun-furat/)

<sup>2</sup> National Renewable Energy Laboratory, 15013 Denver W Parkway,  
Golden, CO 80401, USA

**Abstract.** Microscopy techniques like X-ray computed tomography (CT) or scanning electron microscopy (SEM) can provide detailed image data of the nano- and microstructure of functional materials at various scales. This allows for the investigation of structure-property relationships, i.e., how the nano-/microstructure influences material properties like electrochemical behavior. However, the structural characterization by means of measured image data often entails nontrivial processing tasks. In this paper, a workflow is shown for the holistic structural characterization of active material (AM) particles in Li-ion battery electrodes by means of stochastic modeling. For this purpose, image data is acquired at different length scales and with various measurement techniques, namely, CT, SEM, and focused ion beam (FIB) combined with electron backscatter diffraction (EBSD). To enable quantitative structural characterization through spatial stochastic modeling, machine learning methods for segmentation purposes are initially deployed. Then, a stochastic-geometry model for AM particles is calibrated to image data, overcoming the limitations of the different measurements (e.g., resolution vs. field of view). The model is fitted using CT data for the outer shell of AM particles and FIB-EBSD data for the polycrystalline grain architecture within. Then, the model is used to perform structural scenario analyzes, i.e., to generate numerous digital twins with statistically similar shape and grain architecture as observed in measured image data. These digital twins are input for numerical (dis)charging simulations to investigate their degradation behavior, e.g., AM particle cracking due to repeated cycling.

**Keywords:** Stochastic geometry, multi-scale model, machine learning, Li-ion battery electrode, active material particle, digital twin

---

\*OF and LF contributed equally.

## 1 Introduction

To enable widespread electrification of passenger vehicles, lithium-ion batteries must achieve high energy densities, rapid charging capabilities and extended lifespans. The morphology of battery electrodes, especially the 3D nanostructure of individual electrode particles, significantly impacts performance, yet this influence is not fully understood [1]. For example, the most common positive electrode (cathode) material in these batteries, namely  $\text{LiNiMnCoO}_2$  (NMC) particles, have irregular non-spherical shapes and, in addition, exhibit complex internal structures that both affect their functionality. More precisely, cathodes of these batteries are made up of polycrystalline NMC particles, where each crystal (also referred to as grain) facilitates lithium transport along two-dimensional planes. The morphology of the grains themselves as well as their random crystal lattice orientation introduce a level of complexity in lithium paths, leading to mechanical stresses during charging and discharging processes, which can result in particle cracking and faster degradation of the battery's capacity [1–4].

Recent advancements in imaging technologies such as X-ray computed tomography (CT) and the combination of focused ion beam (FIB) with electron backscatter diffraction (EBSD) have significantly enhanced our ability to study these microstructures in three dimensions. In particular, nano- and micro-CT, have proven effective in imaging and quantifying the morphological properties of particles non-destructively, although it falls short in capturing the orientation of individual grains within the particles [5]. FIB-EBSD has filled this capability gap by allowing for precise quantification of both the morphology and orientation of intra-particle grains in 3D, by repeated acquisition of 2D EBSD data followed by removal of the imaged surface by the FIB [6].

For various types of nano/microstructures of different materials, 3D image data has been the basis for deriving spatial stochastic 3D models, i.e., models from which random morphologies can be generated which are statistically similar to imaged nano/microstructures [7]. In particular, when leveraging parametric models, the calibration to image data implies a search for well-fitting parameters. After model fitting, the parameters, which influence the morphology of simulated nano/microstructures can be varied systematically, such that a broad database of differently structured morphologies can be generated [8]. In addition, spatial stochastic models can be calibrated to image data of materials' nano/microstructures at various length scales. In this manner the individual models, which have been calibrated to data of different length scales, can be combined to a multiscale model. For example, in [9] a 3D model has been derived for the outer shell of particles as well as a further model for their inner nanoporous structure. The combination allowed for the generation of particles with statistically similar shapes and inner pore systems.

Such spatial stochastic models can be the basis for investigating the influence of morphology on effective macroscopic material properties (structure-property relationships) by means of computer-based experiments, an approach also referred to as virtual materials testing [8]. More precisely, the simulated nano/microstructures can be used as geometry input for numerical simulations

of effective macroscopic properties (e.g., effective diffusivity). Then, these effective properties can be correlated with structural descriptors (e.g., volume fractions, specific surface areas, etc.). In particular, the broad database of differently structured morphologies generated by stochastic 3D models allows for the derivation of quantitative structure-property relationships by means of regression analysis with interpretable regression functions or neural networks—which is an important step for material design purposes.

Often, the acquisition of 3D image data is expensive in both time and resources. Many laboratories are equipped with imaging techniques that allow for the acquisition of more accessible 2D image data. However, the statistical analysis of 3D morphologies observed in 2D image data (e.g., planar sections) is often a non-trivial inverse problem [10]. For some types of morphologies, there are theoretical results based on conventional stereological methods that allow for the structural characterization of 3D morphologies from 2D image data. However, for many applications in natural and engineering sciences, conventional methods of stereology cannot be deployed as their requirements are often too restrictive (e.g., some stereological methods rely on the assumption of convex particle shapes). Recently, purely data-driven methods based on generative adversarial networks (GAN) have emerged which allow for the generation of 3D morphologies the planar sections of which are statistically similar to those observed in 2D image data [11]. As these methods are non-parametric, it is difficult to systematically simulate differently structured 3D morphologies. Consequently, GAN-based approaches for modeling 3D morphologies from 2D image data might not be viable for the purpose of virtual materials testing, as described above.

In the present paper, we unify computational methods described in [12, 13], for the calibration of a multi-scale model from which virtual NMC particles in Li-ion battery electrodes can be generated together with their inner grain architecture, see Figure 1. As the morphology of their outer shell as well as their inner grain architecture influence the properties of corresponding battery materials, the stochastic 3D model which serves as the basis for virtual materials testing considers both length scales.

## 2 Materials, image acquisition and processing

The materials for which we derive multi-scale models in the present paper are cathode particles in Li-ion batteries. More precisely, common Li-ion battery cathodes are comprised of so-called NMC particles. In this paper, we consider two types of NMC particles, namely,  $\text{LiNi}_{0.5}\text{Mn}_{0.3}\text{Co}_{0.2}\text{O}_2$  (NMC532) and  $\text{LiNi}_{0.8}\text{Co}_{0.1}\text{Mn}_{0.1}\text{O}_2$  (NMC811) particles.

For both type of NMC particles, 3D image data has been acquired by means of X-ray nano-CT. These images exhibit the outer shell of numerous particles which have been segmented into individual particles using the watershed transform, see Figure 1 (bottom left). For more details on the CT image data, its acquisition and pre-processing, the reader is referred to [12, 13].

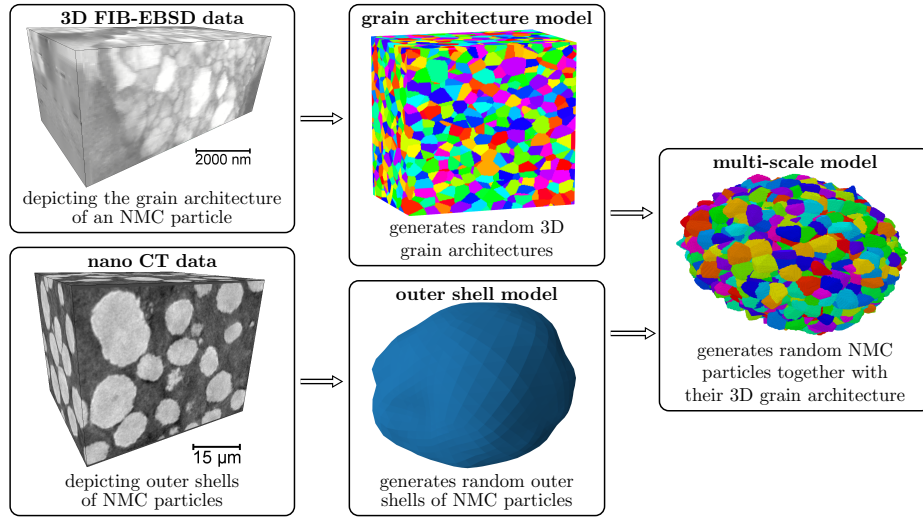


**Fig. 1.** Workflow of fitting stochastic multi-scale models for polycrystalline particles in Li-ion battery cathodes. Top row: A stochastic 3D model is calibrated to FIB-EBSD image data, from which statistically similar grain architectures of NMC particles can be generated. Bottom row: Using 3D nano-CT data a stochastic 3D model is calibrated from which statistically similar outer shells of NMC particles can be generated. Right: By combining both 3D models, a multi-scale model is obtained. Adapted from Figure 1 in [12], licensed under CC BY 4.0 <https://creativecommons.org/licenses/by/4.0>.

Both NMC532 as well as NMC811 particles have a polycrystalline inner structure, i.e., they are comprised of numerous crystals which are also referred to as grains. However, the inner grain architecture cannot be observed in nano-CT data—instead, EBSD imaging can be leveraged. For this purpose, FIB can be used to partially mill away material from a particle. The exposed planar section can then be imaged using EBSD—resulting in 2D image data of the grain architecture. By repeated FIB milling followed by EBSD imaging a stack of 2D images, i.e., 3D image data, of the grain architecture can be acquired. However, the acquisition of 3D EBSD data is expensive in both time and resources, such that it can be favorable to perform modeling using only 2D EBSD data. In the present paper, we consider both scenarios. More precisely, 3D EBSD data of the grain architecture of NMC532 particles and 2D EBSD data of the grain architecture of NMC811 particles are available for the purpose of modeling. Both the 2D and 3D EBSD data has then been segmented into individual grains, see [12, 13] for further details on the acquisition of the image data and its processing.

### 3 Stochastic 3D model for outer particle shells

In this section, we describe a method for calibrating a stochastic 3D model for the outer shell of so-called star-shaped particles. Therefore, let  $P_1, \dots, P_n \subset \mathbb{R}^d$

denote  $n > 0$  particles observed in segmented nano-CT image data. For the purpose of modeling, we first determine an efficient representation for these particles. More precisely, for each  $i \in \{1, \dots, n\}$  we derive a radius function  $r_i: S^2 \rightarrow [0, \infty)$  given by  $r_i(u) = \sup\{\alpha \geq 0: \alpha u \in P_i\}$ , for each (direction) vector  $u \in S^2$ , where  $S^2 \subset \mathbb{R}^3$  denotes the set of all direction vectors, i.e., the surface of the unit sphere in  $\mathbb{R}^3$ . Consequently, the observed particles are now represented by the radius functions  $r_1, \dots, r_n$  which we will model by means of random fields on  $S^2$ .

### 3.1 Random fields on the unit sphere

Formally, a random field on the unit sphere  $S^2 \subset \mathbb{R}^3$  is a collection  $X = \{X(u): u \in S^2\}$  of real-valued random variables. If the values of  $X(u)$  for each  $u \in S^2$  are positive with probability 1, the random field  $X$  can be considered to be a random radius function. Thus, when modeling the outer shell of particles, the goal is to determine a suitable model  $X$  such that the radius functions  $r_1, \dots, r_n$  derived from measured image data are likely to be realizations of  $X$ . In order to make modeling more feasible it is common practice to introduce some model assumptions. When modeling the shape of particles a reasonable assumption is isotropy of  $X$  meaning that the distribution of  $X$  does not change if we rotate the Euclidean coordinate system around the origin  $o \in \mathbb{R}^3$ . The assumption of isotropy, together with the assumption of square integrability of  $X(u)$  for each  $u \in S^2$ , implies a representation of  $X$  that makes modeling more accessible, i.e., the series expansion

$$X(u) = \sum_{\ell=0}^{\infty} \sum_{m=-\ell}^{\ell} a_{\ell m} Y_{\ell m}(u) \tag{1}$$

holds for each  $u \in S^2$ , where  $Y_{\ell m}: S^2 \rightarrow \mathbb{C}$  are so-called spherical harmonic functions with values in the complex plane  $\mathbb{C}$  and  $a_{\ell m}$  are uncorrelated complex-valued random variables [14]. More precisely, the random variables  $a_{\ell m}$  are given by  $a_{\ell m} = \int_{S^2} X(u) \overline{Y_{\ell m}(u)} \mathcal{H}(du)$ , where  $\mathcal{H}$  is the surface measure on  $S^2$ . The coefficients  $a_{\ell m}$  appearing in the series expansion given in Eq. (1) are uncorrelated (with uncorrelated real and imaginary parts) such that  $\mathbb{E}a_{\ell m} = 0$  for each  $\ell > 0$ .

Common statistics of isotropic random fields on  $S^2$  are the mean value  $\mu = \mathbb{E}X(u) \in \mathbb{R}$  (which does not depend on  $u \in S^2$ ) and the covariance function  $C: S^2 \times S^2 \rightarrow \mathbb{R}$  given by

$$C(u, v) = \mathbb{E}[(X(u) - \mu)(X(v) - \mu)] = \sum_{\ell=0}^{\infty} A_{\ell} \frac{2\ell + 1}{4\pi} P_{\ell}(\langle u, v \rangle), \tag{2}$$

where the coefficients  $A_{\ell} \geq 0$  are referred to as angular power spectrum and  $P_{\ell}$  are the Legendre polynomials [15]. Note that the member  $A_{\ell} \geq 0$  of the angular power spectrum is the variance of the coefficient  $a_{\ell m}$  for any  $\ell \geq 0$  and  $m \in \{-\ell, \dots, \ell\}$ .

### 3.2 Model calibration using the maximum likelihood method

Gaussian random fields (GRFs) on  $S^2$  are rather well studied objects, where a random field  $X = \{X(u) : u \in S^2\}$  is called Gaussian if  $(X(u_1), \dots, X(u_m))$  is a (multivariate) normal distributed random vector for any  $m > 0$  and  $u_1, \dots, u_m \in S^2$ . Note that isotropic GRFs on  $S^2$  are uniquely characterized by their mean value  $\mu = \mathbb{E}X(u)$  and angular power spectrum  $A_0, A_1, \dots$ . Due to computational limitations, we set  $A_\ell = 0$  for each  $\ell > L$  and some integer  $L > 0$ . Consequently, with this modeling assumption, GRFs are fully characterized by the parameter vector  $\theta = (\mu, A_0, \dots, A_L) \in \Theta$ , where  $\Theta \subset \mathbb{R} \times [0, \infty)^{L+1}$  is some parameter space. The value of  $\theta$  can be fitted to the radius functions  $r_1, \dots, r_n$  derived from image data, using the maximum likelihood method. Thus, the maximum likelihood estimator  $\hat{\theta}$  of  $\theta$  is computed by maximizing the log-likelihood function, i.e.,

$$\hat{\theta} = \arg \max_{\theta \in \Theta} \sum_{i=1}^n \log(f(r_i(u_1), \dots, r_i(u_m) \mid \theta)), \quad (3)$$

where  $f(\cdot \mid \theta)$  denotes the probability density of  $(X(u_1), \dots, X(u_m))$  given that the underlying GRF  $X$  has the parameter vector  $\theta$ . Then, a GRF  $X$  with parameter vector  $\hat{\theta}$  can be used to generate outer shells which are statistically similar to the outer shells observed in measured image data, see Figure 1 (bottom, right).

Note that we draw samples from a truncated GRF, i.e., we disregard model realizations that have negative values and, consequently, are unrealistic radii functions. Furthermore, note that the maximum likelihood approach explained above can be deployed also for non-Gaussian fields. In particular, in [12], a mixture of Gaussian random fields has been fitted in this manner to image data.

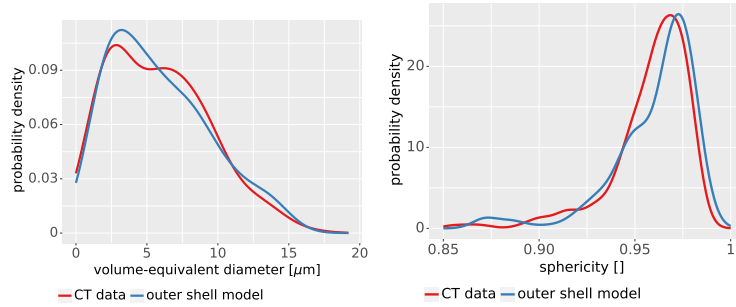


**Fig. 2.** Kernel density estimates of volume-equivalent diameter and sphericity of outer shells observed in image data (red) and generated by the stochastic outer shell model (blue). Adapted from Figure 7 in [12], licensed under CC BY 4.0 <https://creativecommons.org/licenses/by/4.0>

### 3.3 Model validation

We now check the goodness of fit, when fitting a mixture of GRFs to outer shells of NM532 particles observed in nano-CT data. More precisely, after calibrating the model as explained in Section 3.2, we repeatedly draw samples of outer shells from the model for which we compute several morphological descriptors, namely, their volume-equivalent diameter and sphericity. In Figure 2 the probability density of volume-equivalent diameter (left, blue line) and sphericity (right, blue line) of model realizations are visualized. The red lines in Figure 2 depict the corresponding probability densities for outer shells observed in image data—indicating a quite good fit. Similarly, a stochastic outer shell model has been fitted and validated for NMC811 particles, see [13].

## 4 Stochastic 3D model for inner grain architectures

### 4.1 Parametric representation of grain architectures by tessellations

Before explaining the stochastic modeling approach for the grain architecture of polycrystalline materials, we first introduce an efficient representation of such 3D morphologies, where so-called tessellations are used for deriving low-parametric partitionings of a given sampling window  $W \subset \mathbb{R}^3$  into individual cells. By interpreting the cells of a tessellation as grains, a low-parametric representation of grain architectures is achieved, which is more advantageous for modeling purposes than using raw image data. More precisely, we consider so-called generalized balanced power diagrams (GBPDs) [16] whose cells, denoted by  $G_i, i \in \{1, \dots, n\}$  for some integer  $n > 0$ , are given by

$$G_i = \left\{ x \in \mathbb{R}^3 : \sqrt{(x - s_i)^\top m_i (x - s_i)} - r_i \leq \sqrt{(x - s_j)^\top m_j (x - s_j)} - r_j \right\}, \quad (4)$$

where the positive definite matrices  $m_i \in \mathbb{R}^{3 \times 3}$ , the additive weights  $r_i \in \mathbb{R}$  and the so-called seed points  $s_i \in \mathbb{R}^3$  for  $i \in \{1, \dots, n\}$  are the parameters of the tessellation. In general, the cells of a GBPD are non-convex sets. However, by imposing additional constraints on the matrices  $m_i$ , one gets so-called Laguerre tessellations as a special case, the cells of which are convex polyhedra. Depending on the data situation such constraints can be reasonable, since they can simplify subsequent modeling steps [17].

### 4.2 Random tessellations and their simulation

The parameters  $(s_1, m_1, r_1), \dots, (s_n, m_n, r_n)$  of the GBPD extracted from measured image data are used in order to fit a random tessellation, i.e., a stochastic grain architecture model to data. In particular, the sequence  $s_1, \dots, s_n \in \mathbb{R}^3$  of seed points is modelled by a so-called random point process  $\Phi = \{S_1, \dots, S_n\}$ , where  $S_1, \dots, S_n$  are three-dimensional random vectors with values in the sampling window  $W \subset \mathbb{R}^3$ . Moreover, the labels  $(m_1, r_1), \dots, (m_n, r_n)$  of the seed

points  $s_1, \dots, s_n$ , which control the size and shape of the cells  $G_1, \dots, G_n$ , are modeled by a sequence of random vectors  $(M_1, R_1), \dots, (M_n, R_n)$  with values in  $\mathbb{R}^{3 \times 3} \times \mathbb{R}$ . Often, the random vectors  $(M_1, R_1), \dots, (M_n, R_n)$  are assumed to be independent and identically distributed as well as independent of the random point process  $\Phi = \{S_1, \dots, S_n\}$  which models the seed points of cells. However, in some cases, it is reasonable to waive this type of model assumptions and to allow interdependencies between the random variables  $(M_1, R_1), \dots, (M_n, R_n)$  and  $\Phi = \{S_1, \dots, S_n\}$ .

Realizations of the stochastic grain architecture model described above can be generated in the following way. First, a sample is drawn from the point process  $\Phi = \{S_1, \dots, S_n\}$  to generate a point pattern  $\{s_1, \dots, s_n\}$  of seed points. Then, a sample  $(m_1, r_1), \dots, (m_n, r_n)$  is drawn from the (conditional) distribution of the sequence of random labels  $(M_1, R_1), \dots, (M_n, R_n)$ , given a realization  $\{s_1, \dots, s_n\}$  of the point process  $\Phi$  of seed points. In this way, the parameters  $(s_1, m_1, r_1), \dots, (s_n, m_n, r_n)$  of a GBPD are generated which result in the cells  $G_1, \dots, G_n$  according to the rule given in Eq. (4).

The calibration of the random point process  $\Phi$  and the random vectors  $(M_1, R_1), \dots, (M_n, R_n)$  by means of measured 3D and 2D image data is explained in Sections 4.3 and 4.4, respectively.

### 4.3 Model calibration by means of 3D image data

If 3D image data is available, the stochastic grain architecture model described above can be calibrated as follows. First, seed points  $s_i$  and labels  $(m_i, r_i)$  of a (deterministic) GBPD are fitted to measured 3D image data such that the discrepancy between the grains observed in measured image data and their representation as cells of a tessellation are minimized [17]. Then, in a second step, the seed points and their labels are modeled stochastically, i.e., the distribution of a random point process  $\Phi = \{S_1, \dots, S_n\}$  (e.g., a Poisson point process or a Matérn cluster processes) is fitted to the seed points, and the (joint) distribution of the random vectors  $(M_1, R_1), \dots, (M_n, R_n)$  is fitted to the labels. As already stated in Section 4.2, the random vectors  $(M_1, R_1), \dots, (M_n, R_n)$  can depend on local features of the point process  $\Phi = \{S_1, \dots, S_n\}$ , e.g., the random label  $(M_i, R_i)$  of  $S_i$  can depend on the distance to the nearest neighboring seed point. Then, to capture such dependencies, so-called copulas are used in order to model multivariate probability distributions of random vectors with correlated non-Gaussian components, see [12] for further details.

### 4.4 Stereological model calibration based on 2D image data

If only 2D image data is available, the method described in Section 4.3 cannot be deployed for calibrating stochastic grain architecture models in 3D. Instead, the following stereological approach can be used which combines methods of machine learning and spatial stochastic modeling. Therefore, let  $\Phi$  be a random point process in 3D, whose distribution is characterized by the parameter  $\theta_1 \in \Theta_1 \subset \mathbb{R}^{d_1}$  for some  $d_1 \geq 1$ , and let  $(M_1, R_1), \dots, (M_n, R_n)$  be random vectors,

whose (joint) distribution is characterized by the parameter  $\theta_2 \in \Theta_2 \subset \mathbb{R}^{d_2}$  for some  $d_2 \geq 1$ , where the values of  $\theta_2$  can depend on the realizations of  $\Phi$ .

The goal is to predict the values of  $\theta_1$  and  $\theta_2$  by means of measured 2D image data. For that purpose, for some initial values of  $\theta_1$  and  $\theta_2$ , realizations are drawn from the corresponding stochastic grain architecture model, where virtual planar sections of these realizations are computed and statistically compared with the 2D image data. Then, in the next step, the values of  $\theta_1$  and  $\theta_2$  are successively adapted in order to maximize the statistical similarity between grain morphologies observed in measured and simulated 2D image data. To evaluate this similarity, morphological descriptors are computed for both datasets and statistically compared to each other, where an efficient optimization of the model parameters is achieved by implementing a differentiable statistical comparison rule in the optimization routine. Furthermore, an (almost everywhere differentiable) convolutional neural network is used to determine the descriptors for the statistical comparison of simulated 2D grain architectures with those of measured image data. This results in a generative adversarial network-based training procedure, see [13] for further details.

#### 4.5 Model validation

To give an example, we discuss the quality of the fitted (deterministic and stochastic) grain architecture models for NMC532 particles, where a random Laguerre tessellation has been calibrated by means of 3D EBSD data using the method described in Section 4.3. Figure 3 (red, blue) shows that the cells of the deterministic Laguerre tessellation fitted to measured image data, as stated in Section 4.1, accurately reflects the grain architecture observed in image data (in terms of volume-equivalent diameter and sphericity), making it a reasonable model restriction over more general GBPDs. Moreover, Figure 3 shows that the distributions of volume-equivalent diameter and sphericity of simulated cells (green) drawn from a random Laguerre tessellation and grains in image data also match quite well.

### 5 Stochastic 3D multi-scale model

The outer shell and inner grain architecture of the NMC particles considered in this paper are assumed to be independent, especially for larger particles. Thus, to generate a particle with an inner grain architecture, both a simulated grain architecture and a simulated outer shell are independently drawn from the corresponding models stated in Sections 3 and 4, respectively, and then combined. More precisely, grains whose centers of masses do not lie within the outer shell are removed. Figure 1 (right) illustrates the result obtained by this procedure, showing samples drawn from the outer shell model, the grain architecture model, and their combination into a simulated NMC particle.

The stochastic multi-scale model explained above has been used to generate several differently structured virtual NMC particles for the purpose of virtual materials testing. For example, in [1], the virtual NMC particles served

as geometry input for simulating lithium diffusion during battery charging and discharging and the resulting chemo-mechanical stress/strains. In this manner, the influence of particle nano/microstructure on structural degradation and on chemo-mechanically induced capacity loss can be investigated.

## 6 Conclusion

We presented a computational framework for data-driven stochastic modeling the outer shell of  $\mu\text{m}$ -sized particles together with their inner polycrystalline grain architecture in 3D—resulting in a multi-scale model which characterizes the 3D morphology of such particles at different length scales. Polycrystalline particles of this type occur, for example, in cathodes of Li-ion batteries. Our modeling approach complements the advantages of different imaging techniques like nano-CT and EBSD rather well. On the one hand, nano-CT does not provide information on the grain architecture, yet provides image data of numerous NMC particles in 3D. On the other hand, grains are observable in EBSD data, yet the acquisition of 3D data as well as the imaging of numerous NMC particles can be difficult. Thus, the presented modeling approach overcomes the limitations of both imaging techniques as it allows for the generation of arbitrarily many virtual NMC particles with inner grain architecture, which are nicely mimicking the 3D morphology of real NMC particles and, therefore, can serve as a basis for virtual materials testing.

For modeling the 3D morphology of these particles, two types of spatial stochastic models were presented. The first one is a random field model for the outer shell of particles, i.e., the size and shape of particles. The second model are random tessellations which can, after calibration, generate statistically similar grain architectures as observed in measured image data. For the purpose of model calibration, we describe two approaches, which rely either on 3D or 2D image data of the grain architecture. Note that the presented computational methods are relatively independent of both material and length scale, such that they can be transferred to other applications than battery electrodes relatively easily. Moreover, the ability to calibrate a 3D model on the basis of 2D image data, i.e., to achieve a statistical 3D reconstruction, can significantly reduce measurement costs both in time and resources.

The focus of our future work will be to transfer the methodology, presented in this paper for statistically reconstructing 3D morphologies from 2D data, to further types of advanced structural materials. Moreover, the multi-scale models for NMC particles will be extended with respect to a further important aspect—namely, cracking which occurs on various length scales within such particles due to chemo-mechanical stress/strains. This structural degradation of battery materials has been investigated by means of 2D image data, which, however, does not directly allow for the quantitative analysis of transport path lengths in 3D [3, 18]. We will introduce a stochastic 3D crack model which is based on the multi-scale models described in the present paper—i.e., by simulating cracks along interfaces of neighboring grains (grain boundaries), see also [19]. Moreover,

the stochastic 3D crack model will be calibrated by means of 2D image data. Consequently, transport path lengths and further geometrical descriptors that are relevant for battery performance, but unobservable in 2D image data, can be computed from 3D morphologies generated by the model.

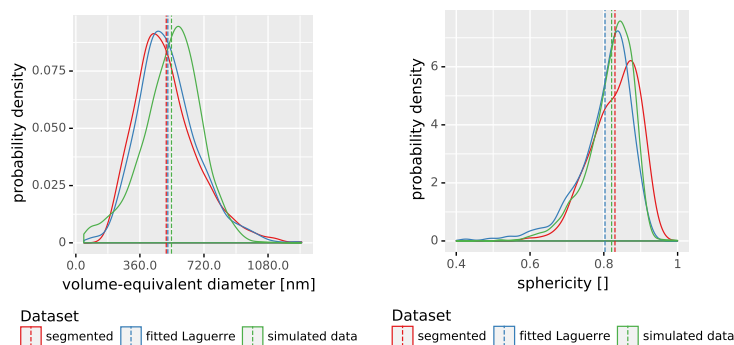


**Fig. 3.** Kernel density estimates of volume-equivalent diameter and sphericity of grains observed in measured image data (red), cells of fitted Laguerre tessellation (blue), and simulated cells (green) drawn from random Laguerre tessellation. Vertical lines indicate mean values. Adapted from Figure 9 in [12], licensed under CC BY 4.0 <https://creativecommons.org/licenses/by/4.0>

## References

- Allen, J. M., Weddle, P. J., Verma, A., Mallarapu, A., Usseglio-Viretta, F., Finegan, D. P., Colclasure, A. M., Mai, W., Schmidt, V., Furat, O., Diercks, D., Tanim, T., Smith, K.: Quantifying the influence of charge rate and cathode-particle architectures on degradation of Li-ion cells through 3D continuum-level damage models. *J. Power Sources* 512, 230415 (2021). doi: 10.1016/j.jpowsour.2021.230415
- Quinn, A., Moutinho, H., Usseglio-Viretta, F., Verma, A., Smith, K., Keyser, M., Finegan, D. P.: Electron backscatter diffraction for investigating lithium-ion electrode particle architectures. *Cell Rep. Phys. Sci.* 1(8), 100137 (2020). doi: 10.1016/j.xcrp.2020.100137
- Furat, O., Finegan, D. P., Yang, Z., Tanim, T. R., Smith, K., Schmidt, V.: Quantifying the impact of charge rate and number of cycles on structural degeneration of Li-ion battery electrodes. *J. Electrochem. Soc.* 169(10), 100541 (2022). doi: 10.1149/1945-7111/ac99a1
- Chen, W.-X., Allen, J. M., Rezaei, S., Furat, O., Schmidt, V., Singh, A., Weddle, P. J., Smith, K., Xu, B.-X.: Cohesive phase-field chemo-mechanical simulations of inter- and trans-granular fractures in polycrystalline NMC cathodes via image-based 3D reconstruction. *J. Power Sources* 596, 234054 (2024). doi: 10.1016/j.jpowsour.2024.234054
- Heenan, T. M. M., Wade, A., Tan, C., Parker, J. E., Matras, D., Leach, A. S., Robinson, J. B., Llewellyn, A., Dimitrijevic, A., Jervis, R., Quinn, P. D., Brett, D. J. L., Shearing, P. R.: Identifying the origins of microstructural defects such as

- cracking within Ni-rich NMC811 cathode particles for lithium-ion batteries. *Adv. Energy Mater.* 10, 2002655 (2020). doi: 10.1002/aenm.202002655
6. Furat, O., Finegan, D. P., Diercks, D., Usseglio-Viretta, F., Smith, K., Schmidt, V.: Mapping the architecture of single electrode particles in 3D, using electron backscatter diffraction and machine learning segmentation. *J. Power Sources* 483, 229148 (2021). doi: 10.1016/j.jpowsour.2020.229148
  7. Chiu, S. N., Stoyan, D., Kendall, W. S., Mecke, J.: *Stochastic Geometry and Its Applications*. J. Wiley & Sons (2013)
  8. Prifling, B., Rödning, M., Townsend, P., Neumann, M., Schmidt, V.: Large-scale statistical learning for mass transport prediction in porous materials using 90,000 artificially generated microstructures. *Front. Mater.* 8, 786502 (2021). doi: 10.3389/fmats.2021.786502
  9. Neumann, M., Wetterauer, S. E., Osenberg, M., Hilger, A., Gräfensteiner, P., Wagner, A., Bohn, N., Binder, J. R., Manke, I., Carraro, T., Schmidt, V.: A data-driven modeling approach to quantify morphology effects on transport properties in nanostructured NMC particles. *Int. J. Solids. Struct.* 280, 112394 (2023). doi: 10.1016/j.ijsolstr.2023.112394
  10. Baddeley, A., Jensen, E. B. V.: *Stereology for Statisticians*. Chapman and Hall (2004)
  11. Kench, S., Cooper, S. J.: Generating three-dimensional structures from a two-dimensional slice with generative adversarial network-based dimensionality expansion. *Nat. Mach. Intell.* 3(4), 299–305 (2021). doi: 10.1038/s42256-021-00322-1
  12. Furat, O., Petrich, L., Finegan, D. P., Diercks, D., Usseglio-Viretta, F., Smith, K., Schmidt, V.: Artificial generation of representative single Li-ion electrode particle architectures from microscopy data. *npj Comput. Mater.* 7(1), 105 (2021). doi: 10.1038/s41524-021-00567-9
  13. Fuchs, L., Furat, O., Finegan, D. P., Allen, J., Usseglio-Viretta, F. L. E., Ozdogru, B., Weddle, P. J., Smith, K., Schmidt, V.: Generating multi-scale NMC particles with radial grain architectures using spatial stochastics and GANs. *arXiv preprint* (2024). doi: 10.48550/arXiv.2407.05333
  14. Marinucci, D., Peccati, G.: *Random Fields on the Sphere: Representation, Limit Theorems and Cosmological Applications*. Cambridge University Press (2011)
  15. Abramowitz, M., Stegun, I. A.: *Handbook of Mathematical Functions with Formulas, Graphs, and Mathematical Tables*. Dover Publications, Inc. (1970)
  16. Alpers, A., Brieden, A., Gritzmam, P., Lyckegaard, A., Poulsen, H. F.: Generalized balanced power diagrams for 3D representations of polycrystals. *Phil. Mag.* 95(9), 1016–1028 (2015). doi: 10.1080/14786435.2015.1015469
  17. Petrich, L., Furat, O., Wang, M., Krill III, C. E., Schmidt, V.: Efficient fitting of 3D tessellations to curved polycrystalline grain boundaries. *Front. Mater.* 8, 760602 (2021). doi: 10.3389/fmats.2021.760602
  18. Furat, O., Finegan, D. P., Yang, Z., Neumann, M., Kim, S., Tanim, T. R., Weddle, P., Smith, K., Schmidt, V.: Quantifying the impact of operating temperature on cracking in battery electrodes, using super-resolution of microscopy images and stereology. *Energy Storage Mater.* 64, 103036 (2024). doi: 10.1016/j.ensm.2023.103036
  19. Rieder, P., Furat, O., Weddle, P., Allen, J., Finegan, D. P., Smith, K., Schmidt, V.: Methods of machine learning and stochastic modeling for the structural characterization of functional battery materials at various length scales. In: *Book of Abstracts of the 20th Symposium on Modeling and Experimental Validation of Electrochemical Energy Technologies*, p. 129. Baden, Switzerland (2024). doi: 10.3929/ethz-b-000662523